Journal of Materials Science & Technology 98 (2022) 244–247

Contents lists available at ScienceDirect

Journal of Materials Science & Technology

journal homepage: www.elsevier.com/locate/jmst

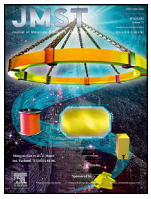

Letter

Achieving high hetero-deformation induced (HDI) strengthening and hardening in brass by dual heterostructures

Heterostructured materials, defined as materials that contain multiple zones with dramatically different flow stresses, have the potential to push the envelope of the strength-ductility of metals and alloys beyond what can be obtained conventionally [1–3]. A prominent example is the heterogeneous lamella Ti that is as strong as its ultrafine-grained Ti, while as ductile as the coarse-grained Ti [4]. The superior properties of heterostructured materials were attributed to the significant development of hetero-deformation induced (HDI) strengthening and hardening [2,5,6]. Besides the heterogeneous lamella materials [4,7,8], many other groups of materials with diverse microstructures can also be considered as heterostructured materials, including bimodal materials [9,10], gradient materials [11,12], harmonic structure materials [13,14], dual-phase steels [15,16], and laminated materials [17,18].

Single-type heterostructure has hitherto been the central theme of most studies because of the need to investigate each structural parameter that affects the HDI hardening [7,9,17,19]. A combination of different heterostructures, or the hierarchical design of heterostructures, may offer the potential to further improve strength and ductility [20]. A few recent experimental studies, employing combinations of heterostructures, revealed encouraging results. Wu et al. [21] and Guo et al. [22] superimposed the phase-transformation heterostructure on the grain-size gradient structure in stainless steel to obtain enhanced yield strength and uniform elongation. The hierarchy of heterogeneity has also been proposed to account for the extraordinary properties of high-entropy alloys by elevating the strain hardening using a variety of heterostructures at different length scales [20]. The design of the hierarchy of heterostructures appears promising, yet there is a critical lack of experimental investigation to answer the fundamental questions: (a) Whether the hierarchy of heterostructures outperforms its individual constituents; (b) If so, what is the mechanistic origin for such outperformance? This work aims to fill this knowledge gap using a case study that presents a direct comparison on mechanical properties, microstructural characteristics and hardening behaviors of a hierarchy of heterostructures (dual heterostructures in this work specifically) and its individual heterostructure components.

In this study, a commercial ASM-C26000 alloy (Cu-30wt%Zn) plate was annealed at 700 °C for 2 h to produce a homogeneous coarse-grained (CG) structure. The CG plates were rolled from 10 to 2 mm (80% thickness reduction), with each pass producing ~5% thickness reduction. Subsequently, the rolled brass plate was annealed at 260 °C for 25 min ("PA") to form a heterogeneous lamella structure (HLS). Rotationally accelerated shot peening (RASP) [23], which produces much higher impact energy compared to conventional shot peening, was conducted on the HLS brass samples with a velocity of 30 m/s for 15 min afterward on both sides. In parallel, a CG plate with 2-mm thickness was processed at the same speed and duration on both sides. As such, five groups of samples were made, designated according to their processing and microstructures: (1) rolling to 80% thickness reduction (R80); (2) rolling to 80% thickness reduction + partial annealing (PA), representing the single-type heterogeneous lamella structure; (3) rolling to 80% thickness reduction + partial annealing + RASP (PA+RASP), representing the dual heterostructures where the heterogeneous lamella structure is embedded into a gradient structure; (4) coarse grains (CG); (5) coarse grains + RASP (RASP), representing the single-type gradient structure. Direct comparison among these groups will explicate the role of the dual heterostructure in mechanical properties.

Dog-bone-shaped tensile samples with gauge dimensions of $10 \times 2 \times 2$ mm^3 were tested under uniaxial tension on a Shimadzu AGS machine. Both conventional and loading-unloading-reloading (LUR) tensile tests were carried out at room temperature at a strain rate of ~ 5×10^{-4} s^{-1}, and each test was repeated on at least 5 samples to ensure data reproducibility. Hardness was measured by a Bruker Hysitron TI980 Triboindenter, and hardness at the same depth was repeated 5 times. Microstructures were characterized by an FEI Quanta 3D FEG scanning electron microscope (SEM) with ion channeling contrast microscopy (ICCM) and electron backscattered diffraction (EBSD), and an FEI Talos transmission electron microscope (TEM) operated at 200 kV. Dislocation densities were estimated from X-ray diffraction (XRD) data based on Williamson-Hall methods [24] (Details of methodology and analysis for dislocation density calculation are provided in *supplementary material*).

Fig. 1(a) shows the uniaxial tensile testing results of the five groups of samples. The PA+RASP sample exhibits the best combination of strength and ductility, with ~ 670 MPa yield stress and ~6.5 % uniform elongation. In the strength-ductility Ashby plot (Fig. 1(c)), the PA+RASP (dual heterostructures) sits beyond the bound sketched by all other samples, including the two single-type heterostructures. This result lends direct support to the advantage of the dual heterostructures over its components in the overall mechanical performance. The superior combination of strength and ductility is inherently related to the elevated strain hardening capacity in the sample. As provided in Fig. 1(b), the strain hardening rate of the PA+RASP sample is appreciably higher than samples with either single-type heterostructure, especially during the early plastic stage (< ~3.5%). It has been documented in the early works that the HDI hardening dictates the strain hardening in this strain range, with geometrically necessary dislocations (GNDs) piling up at hard/soft zone boundaries to accommodate the plastic strain gradient [5,7,8]. Therefore, the dual heterostructure appears to exhibit higher HDI hardening than its individual counterparts.

https://doi.org/10.1016/j.jmst.2021.03.088

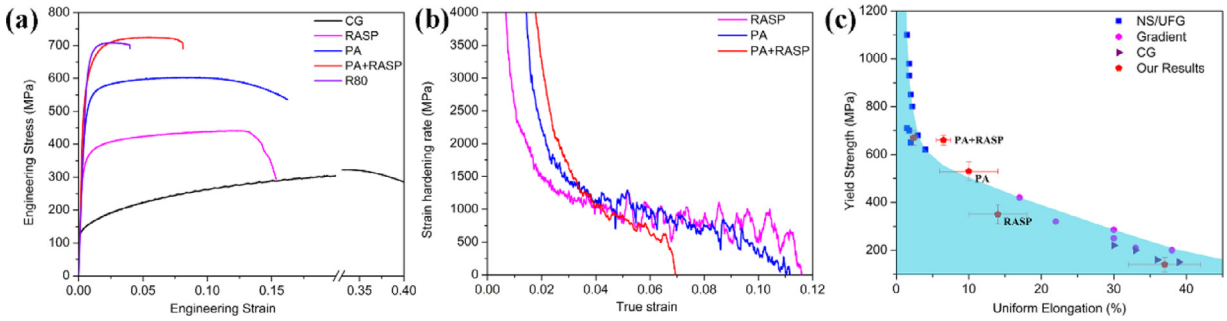

Fig. 1. (a) Strain-stress curves of the samples fabricated by different processing routes; (b) Strain hardening rate curves of the samples; (c) Comparison of mechanical properties of brass samples with different structures [25–29].

To explore the origin of the higher HDI hardening, we firstly characterized the microstructure of the dual heterostructure (PA+RASP sample), with an emphasized comparison to the simple gradient structure (RASP sample). The simple gradient structure in the RASP (Fig. 2(a)) is composed of three different layers with gradient distribution of grain size from the top surfaces to the center: nanograin/ultrafine grain (NG/UFG), deformed CG, and CG [11].

The microstructure of the PA+RASP sample (Fig. 2(b)) is approximately composed of three layers as well. The characteristics of those layers, though, are more complicated than gradient structure superimposed on the heterogeneous lamella structure. The top surface, ~50 μm deep, is comprised of NG/UFG grains (illustrated by Fig. 2(c) and (d)). It bears a strong resemblance to its counterpart in the RASP sample [29]. The second layer is the deformed HLS layer, which is unique in the dual heterostructure, as labeled in Fig. 2(b). It preserves the heterogeneous lamella character from the PA condition to a certain extent while subjected to deformation during the subsequent RASP. The microstructures obtained by EBSD demonstrate such characteristics by comparing the second layers at a similar depth in both RASP and PA+RASP samples (Fig. 2(e) and (f)). The former has a uniform, much coarser and less deformed grain structure, while the latter exhibits a lamellar-like microstructure featured by the alternating well-indexed and non-indexed layers. The partial microstructure's low indexability is not a surprise, mainly due to the much finer grain size and the high residual strain.

To reveal the local microstructure in detail beyond the limitation of EBSD, further TEM investigation of both samples at the same depth was conducted (Fig. 2(g) and (h)). Distinctive microstructural characteristics were observed. The deformed CG layer in the RASP sample exhibits profuse twins, further segmented by the high density of dislocations, as usually observed in low strain regions in gradient materials with low stacking fault energies [30]. In contrast, the deformed HLS layer preserved the heterogeneous lamella structure in general, while further strain-induced subgrain formation is also evidenced in the soft zone (Fig. 2(h)). During the RASP procedure on the PA sample, extensive strain partitioning is expected to occur at the soft/hard zone boundaries, producing dense dislocations and subgrains in the soft zone grains [31]. The high dislocation density at the zone boundaries, along with the HLS, is not available in either conventional grain-size gradient structure or HLS structure alone. It will affect mechanical behavior in its own way, as discussed later. Lastly, the core layer of the PA+RASP sample is the conventional HLS, which has been well studied in Ref. [7] and thus will not be detailed here.

In light of the microstructural characteristics in different samples, we next studied the site-specific hardening behaviors in all of them. Fig. 3(a) is the hardness profile of the as-processed PA+RASP, RASP and PA samples. As shown, there is a unique hardness plateau at ~100 μm in the PA+RASP sample, corresponding to the aforementioned deformed HLS layer. The hardness plateau can be ascribed to the microstructure saturation in both disloca-

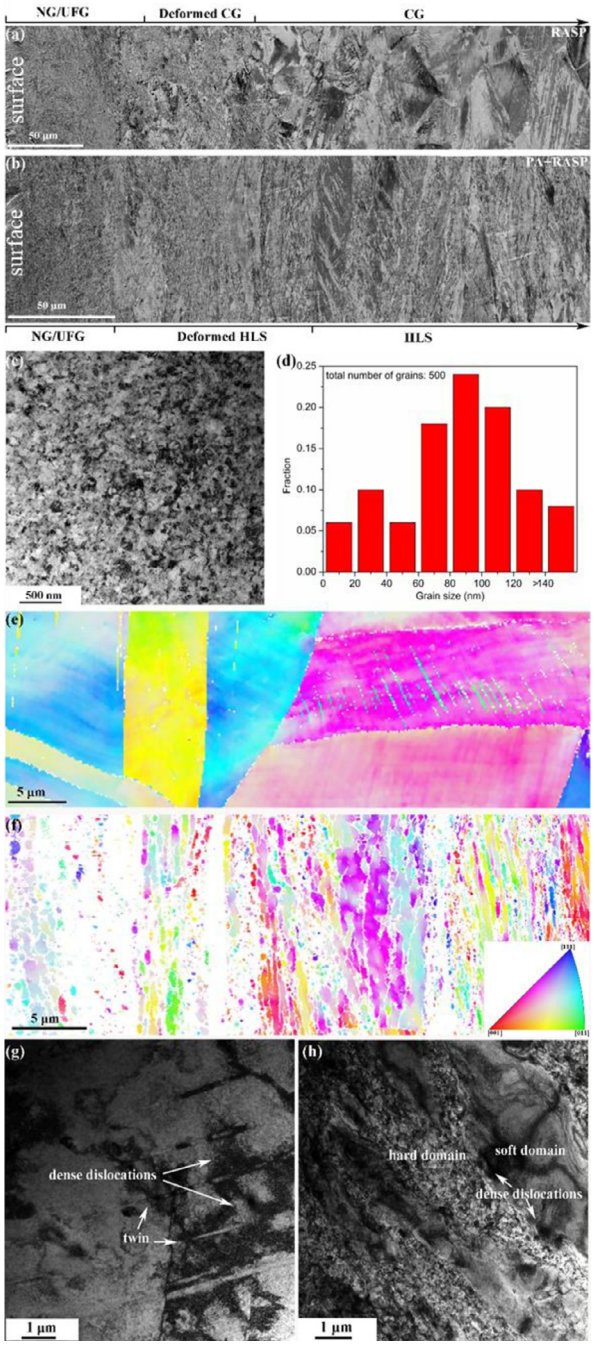

Fig. 2. Representative microstructure starting from surface (a) RASP and (b) PA+RASP samples; (c) and (d) TEM image of the nano/ultrafine layer of PA+RASP samples (< 30 μm) and grain size statistic of the nano/ultrafine layer; EBSD image of (e) RASP and (f) PA+RASP at depth ~ 100 μm; TEM image of (g) RASP and (h) PA+RASP at depth ~ 100 μm.

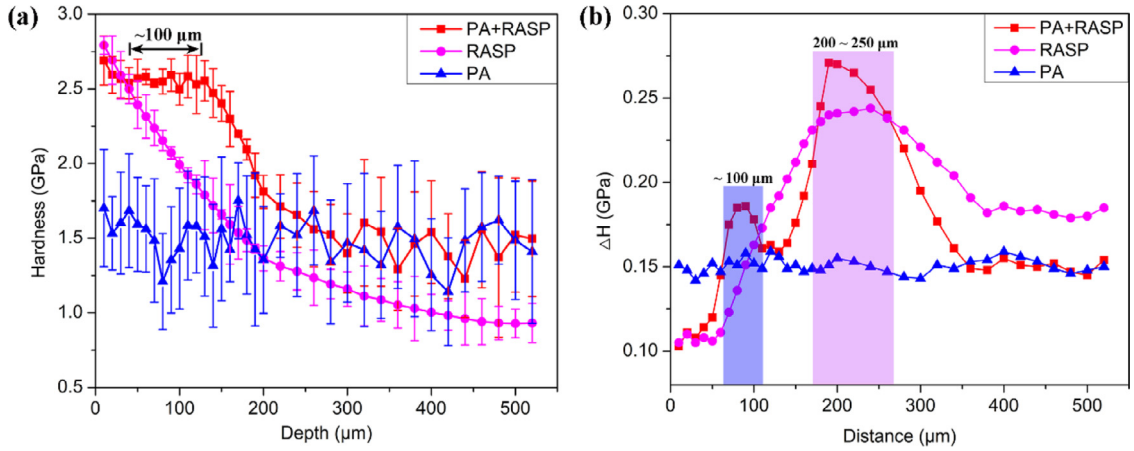

Fig. 3. (a) Hardness profile of three different samples; (b) Increment of hardness after 3% of tensile plastic deformation (the shaded area indicates the peak of the hardness profile).

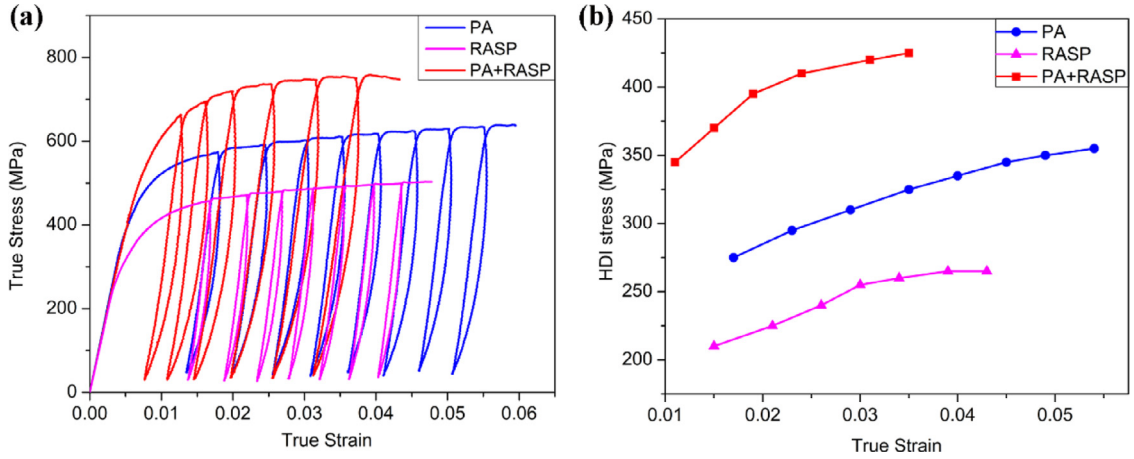

Fig. 4. (a) Loading-unloading-reloading (LUR) test to measure the HDI stresses. (b) HDI stress calculated from the LUR curves.

tion density and grain refinement in the topmost layer, enabled by the combined treatment of PA and RASP. The higher hardness compared to the core should be associated with the high dislocation density in the layer. Notably, the plateau appears to generate two extra relatively sharp interfaces, in addition to the overall gradient from the top surface (~2.7 GPa) to the interior (~1.5 GPa). The two extra sharp interfaces caused by the deformed HLS layer make the dual heterostructure distinctively different from either the smooth gradient or the pure heterogeneous lamellar structure, which could be associated with the extra HDI hardening. We evaluated the hardening capacity by measuring the hardness increase (ΔH) after 3% overall tensile strain. As shown by the shaded regions in Fig. 3(b), while only one blunt peak emerges at ~ 250 μm in the RASP sample as reported in early studies [11], the PA+RASP sample exhibits double sharp peaks of ΔH at both ~ 100 and ~ 250 μm. Notably, the peak values in the PA+RASP sample is also higher than the ΔH at the same depths in the RASP sample. We hypothesize that the observed higher ΔH (hardening) at two peaks are attributed to the extra HDI hardening at the two sharp interfaces in the PA+RASP sample (as indicated in Fig. 3(a)), which plays a crucial role in achieving the enhanced strength and ductility in Fig.1(c) [12].

The total dislocation density increment estimated by XRD (Table 1) lends further support to our hypothesis. The dislocation density increase is higher at the peak locations in the RASP sample, suggesting that Taylor hardening is not responsible for the higher hardening for those sites. Rather, the extra sharp interfaces would generate more GND pile-ups and higher HDI hardening. Their contribution cannot be simply described as Taylor hardening (dislocation hardening) [7], and effectively elevates the overall hardening at early plastic deformation in the PA+RASP samples.

Table 1.
Dislocation density increment at 3% tensile strain ($\times$ 10^{14} m^{-2}).

Depth	PA+RASP	RASP
~100 μm	0.76	1.77
~250 μm	2.70	4.42

The HDI stress measurement through LUR tests [7,32] in Fig. 4 provides further support to the above argument. At the early plastic deformation stage ($<$ ~3% true strain), the HDI hardening rate (the slope of the HDI stress curve) of the PA+RASP sample is higher than that in RASP or PA samples. Hence, the dual heterostructures are more effective than each single-type heterostructure in promoting the piling-up of GNDs. We also note that the HDI hardening becomes weaker in all samples at the later stage, which is because the dislocation interactions made it more challenging to further accumulate GNDs effectively at zone boundaries. Meanwhile, dislocation hardening will finally dominate the total strain hardening in the late stage [7].

Taken as a whole, the PA+RASP sample, combining the HLS and gradient heterostructure, is a basic example of dual heterostructures and demonstrates its advantage in enhancing the strength and ductility over the individual single-type heterostructures that comprise it. Compared to the single-type, the dual heterostructures can generate extra interfaces of heterogeneity, rather than simply piecing different heterogeneity together. The potential of produc-

ing extra heterogeneity beyond its components can leverage the HDI hardening ability and further reduce the trade-off between strength and ductility. This strategy is expected applicable to the design of other heterostructured systems and could be an effective approach to maximize the HDI strengthening and hardening, to design metallic materials with superior mechanical properties.

In summary, a dual heterostructure that includes both HLS and gradient structure was designed in brass, fabricated by rolling, partial annealing and RASP (PA+RASP). Three layers compose the structure: NS/UFG, deformed HLS and core HLS. The deformed HLS becomes a unique layer with two extra sharp interfaces, promoting the HDI hardening. Therefore, the PA+RASP brass has achieved extraordinary HDI strengthening and hardening, compared with its single-type heterostructure constituents, which overcomes the strength-ductility trade-off in the brass. This strategy could be used to design other types of dual or multi-heterostructures for superior mechanical properties.

Declaration of Competing Interest

The authors declare that they have no known competing financial interests or personal relationships that could have appeared to influence the work reported in this paper.

Acknowledgments

This project was supported by the US Army Research Office [W911 NF-12-1-0009]. H. Y. W and Y. Z acknowledged financial support from the National Science Foundation (NSF) under award no. 1929646. EBSD, TEM and XRD characterization were performed in part at the AIF facility, which is supported by the State of North Carolina and the National Science Foundation [ECCS-1542015]. The AIF is a member of the North Carolina Research Triangle Nanotechnology Network (RTNN), a site in the National Nanotechnology Coordinated Infrastructure (NNCI).

Supplementary materials

Supplementary material associated with this article can be found, in the online version, at doi:10.1016/j.jmst.2021.03.088.

References

[1] X. Wu, Y. Zhu, Mater. Res. Lett. 5 (2017) 527–532.
[2] Y. Zhu, X. Wu, Mater. Res. Lett. 7 (2019) 393–398.
[3] Y. Zhu, K. Ameyama, P.M. Anderson, I.J. Beyerlein, H. Gao, H.S. Kim, E. Lavernia, S. Mathaudhu, H. Mughrabi, R.O. Ritchie, N. Tsuji, X. Zhang, X. Wu, Mater. Res. Lett. 9 (2021) 1–31.
[4] X. Wu, M. Yang, F. Yuan, G. Wu, Y. Wei, X. Huang, Y. Zhu, Proc. Natl. Acad. Sci. 112 (2015) 14501–14505.
[5] Y.F. Wang, C.X. Huang, X.T. Fang, H.W. Höppel, M. Göken, Y.T. Zhu, Scr. Mater. 174 (2020) 19–23.
[6] Y.F. Wang, M.S. Wang, X.T. Fang, F.J. Guo, H.Q. Liu, R.O. Scattergood, C.X. Huang, Y.T. Zhu, Int. J. Plast. 123 (2019) 196–207.
[7] X.T. Fang, G.Z. He, C. Zheng, X.L. Ma, D. Kaoumi, Y.S. Li, Y.T. Zhu, Acta Mater. 186 (2020) 644–655.
[8] Z.K. Li, X.T. Fang, Y.F. Wang, P. Jiang, J.J. Wang, C.M. Liu, X.L. Wu, Y.T. Zhu, C.C. Koch, Mater. Sci. Eng. A (2020) 139074.
[9] Y. Wang, M. Chen, F. Zhou, E. Ma, Nature 419 (2002) 912–915.
[10] B.O. Han, E.J. Lavernia, Z. Lee, S. Nutt, D. Witkin, Metall. Mater. Trans. A 36 (2005) 957–965.
[11] T.H. Fang, W.L. Li, N.R. Tao, K. Lu, Science 331 (2011) 1587–1590.
[12] X. Wu, P. Jiang, L. Chen, F. Yuan, Y.T. Zhu, Proc. Natl. Acad. Sci. 111 (2014) 7197–7201.
[13] Z. Zhang, S.K. Vajpai, D. Orlov, K. Ameyama, Mater. Sci. Eng. A 598 (2014) 106–113.
[14] S.K. Vajpai, M. Ota, T. Watanabe, R. Maeda, T. Sekiguchi, T. Kusaka, K. Ameyama, Metall. Mater. Trans. A 46 (2015) 903–914.
[15] K. Park, M. Nishiyama, N. Nakada, T. Tsuchiyama, S. Takaki, Mater. Sci. Eng. A 604 (2014) 135–141.
[16] M. Calcagnotto, Y. Adachi, D. Ponge, D. Raabe, Acta Mater. 59 (2011) 658–670.
[17] X. Ma, C. Huang, J. Moering, M. Ruppert, H.W. Höppel, M. Göken, J. Narayan, Y. Zhu, Acta Mater. 116 (2016) 43–52.
[18] C.X. Huang, Y.F. Wang, X.L. Ma, S. Yin, H.W. Höppel, M. Göken, X.L. Wu, H.J. Gao, Y.T. Zhu, Mater. Today 21 (2018) 713–719.
[19] X. Fang, G. He, M. Ruiz, C. Zheng, Y. Wang, Z. Li, Y. Zhu, Lett. Mater. 9 (2019) 556–560.
[20] E. Ma, X. Wu, Nat. Commun. 10 (2019) 5623.
[21] X.L. Wu, M.X. Yang, F.P. Yuan, L. Chen, Y.T. Zhu, Acta Mater. 112 (2016) 337–346.
[22] N. Guo, Z. Zhang, Q. Dong, H. Yu, B. Song, L. Chai, C. Liu, Z. Yao, M.R. Daymond, Mater. Des. 143 (2018) 150–159.
[23] X. Wang, Y.S. Li, Q. Zhang, Y.H. Zhao, Y.T. Zhu, J. Mater. Sci. Technol. 33 (2017) 758–761.
[24] D. Song, G. Wang, Z. Zhou, E.E. Klu, B. Gao, A. Ma, Y. Wu, J. Sun, J. Jiang, X. Ma, Mater. Sci. Eng. A 773 (2020) 138880.
[25] H. Bahmanpour, K.M. Youssef, J. Horky, D. Setman, M.A. Atwater, M.J. Zehetbauer, R.O. Scattergood, C.C. Koch, Acta Mater. 60 (2012) 3340–3349.
[26] J.R. Davis, ASM Handbook Volume 2: Properties and Selection: Nonferrous Alloys and Special-Purpose Materials, Materials Park, ASM International, Ohio, 2000.
[27] B. Cai, X. Ma, J. Moering, H. Zhou, X. Yang, X. Zhu, Mater. Sci. Eng. A 626 (2015) 144–149.
[28] G.H. Xiao, N.R. Tao, K. Lu, Mater. Sci. Eng. A 513–514 (2009) 13–21.
[29] Y.F. Wang, C.X. Huang, M.S. Wang, Y.S. Li, Y.T. Zhu, Scr. Mater. 150 (2018) 22–25.
[30] N. Tao, H. Zhang, J. Lu, K. Lu, Mater. Trans. 44 (2003) 1919–1925.
[31] J.Y. Huang, Y.T. Zhu, H. Jiang, T.C. Lowe, Acta Mater. 49 (2001) 1497–1505.
[32] M. Yang, Y. Pan, F. Yuan, Y. Zhu, X. Wu, Mater. Res. Lett. 4 (2016) 145–151.

X.T. Fang
Department of Materials Science and Engineering, North Carolina State University, Raleigh, NC 27695, USA

Z.K. Li
Department of Materials Science and Engineering, North Carolina State University, Raleigh, NC 27695, USA
Key Laboratory for Anisotropy and Texture of Materials of Ministry of Education, Northeastern University, Shenyang 110819, China

Y.F. Wang
Department of Materials Science and Engineering, North Carolina State University, Raleigh, NC 27695, USA
School of Aeronautics and Astronautics, Sichuan University, Chengdu 610065, China

M. Ruiz
Department of Materials Science and Engineering, North Carolina State University, Raleigh, NC 27695, USA

X.L. Ma*
Department of Materials Science and Engineering, Texas A and M University, College Station, TX 77840, USA

H.Y. Wang, Y. Zhu
Department of Mechanical and Aerospace Engineering, North Carolina State University, Raleigh, NC 27695, USA

R. Schoell
Department of Nuclear Engineering, North Carolina State University, Raleigh, NC 27695, USA

C. Zheng
Department of Nuclear Engineering, North Carolina State University, Raleigh, NC 27695, USA
Science and Technology on Thermostructural Composite Materials Laboratory, Northwestern Polytechnical University, Xi'an 710072, China

D. Kaoumi
Department of Nuclear Engineering, North Carolina State University, Raleigh, NC 27695, USA

Y.T. Zhu*
Department of Materials Science and Engineering, North Carolina State University, Raleigh, NC 27695, USA

*Corresponding authors.
E-mail addresses: xma4@ncsu.edu (X.L. Ma), ytzhu@ncsu.edu (Y.T. Zhu)
Revised 2 March 2021